Journal of Colloid and Interface Science 581 (2021) 928–938

Contents lists available at ScienceDirect

Journal of Colloid and Interface Science

journal homepage: www.elsevier.com/locate/jcis

Regular Article

A colloid chemistry route for the preparation of hierarchically ordered mesoporous layered double hydroxides using surfactants as sacrificial templates

Gábor Varga [a], Zoltán Somosi [b], Zoltán Kónya [c,d], Ákos Kukovecz [d], István Pálinkó [a], Istvan Szilagyi [b,*]

[a] Materials and Solution Structure Research Group, Department of Organic Chemistry, University of Szeged, H-6720 Szeged, Hungary
[b] MTA-SZTE Lendület Biocolloids Research Group, Interdisciplinary Excellence Center, Department of Physical Chemistry and Materials Science, University of Szeged, H-6720 Szeged, Hungary
[c] MTA-SZTE Reaction Kinetics and Surface Chemistry Research Group, H-6720 Szeged, Hungary
[d] Department of Applied and Environmental Chemistry, University of Szeged, H-6720 Szeged, Hungary

GRAPHICAL ABSTRACT

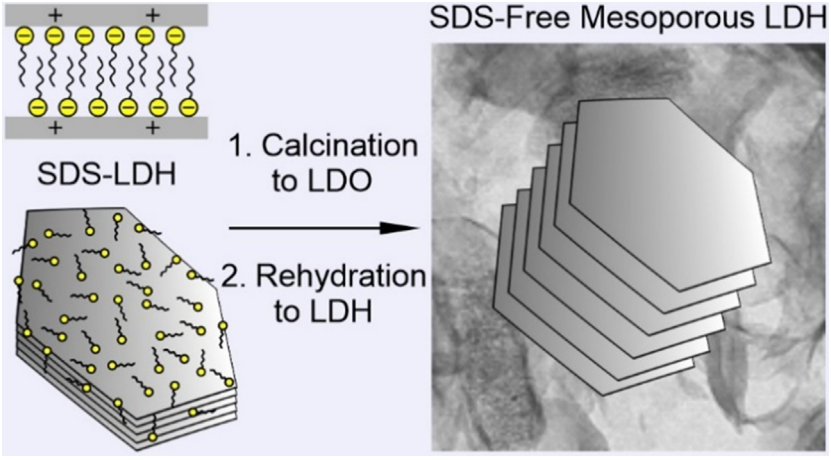

ARTICLE INFO

Article history:
Received 16 July 2020
Revised 19 August 2020
Accepted 28 August 2020
Available online 9 September 2020

Keywords:
Mesoporous layered double hydroxides
Sacrificial template
Colloid stability
Efficient anion removal
SDS-LDH precursor

ABSTRACT

An efficient synthetic route was developed to prepare hierarchically ordered mesoporous layered double hydroxide (LDH) materials. Sodium dodecyl sulfate (SDS) was used as a sacrificial template to tune the interfacial properties of the LDH materials during the synthetic process. The SDS dose was optimized to obtain stable dispersions of the SDS-LDH composites, which were calcined, then rehydrated to prepare the desired LDH structures. Results of various characterization studies revealed a clear relationship between the colloidal stability of the SDS-LDH precursors and the structural features of the final materials, which was entirely SDS-free. A comparison to the reference LDH prepared by the traditional co-precipitation-calcination-rehydration method in the absence of SDS shed light on a remarkable increase in the specific surface area (one of the highest within the previously reported LDH materials) and pore volume as well as on the formation of a beneficial pore size distribution. As a proof of concept, the mesoporous LDH was applied as adsorbent for removal of nitrate and dichromate anions from aqueous samples, and excellent efficiency was observed in both sorption capacity and recyclability. These results

* Corresponding author.
E-mail address: szistvan@chem.u-szeged.hu (I. Szilagyi).

https://doi.org/10.1016/j.jcis.2020.08.118

make the obtained LDH a promising candidate as adsorbent in various industrial and environmental processes, wherever the use of mesoporous and organic content-free materials is required.

1. Introduction

Layered double hydroxide (LDH) materials, also named as hydrotalcites after their naturally occurring form, are lamellar anionic clays, i.e., they possess anion exchange capacity, which is extensively utilized in applications including drug delivery [1], catalysis [2] or environmental remediation [3]. In these processes, one of the critical steps is anion adsorption on the outer surface or in the interlayer space of the oppositely charged LDH layers. The origin of the positive charge can be exemplified by the substitution of magnesium(II) ions with aluminum(III) in the brucite ($Mg(OH)_2$ structure [4], notwithstanding that various divalent and trivalent metal ions were reported as layer forming constituents in LDH structures [5,6].

Towards development of efficient LDH-based anion exchangers of advantageous features for the target applications, several synthetic routes were recommended. The key parameters of such LDHs are the surface charge, specific surface area and pore size distribution, which determine the type of anions preferred for the adsorption/intercalation process. For example, LDH materials of lower surface charge density, but higher pore sizes are good candidates to immobilize and deliver larger biomolecules [7], while high surface charge and area are required for the most efficient anion absorbers in water decontamination [8]. In the latter case, significant effort was made to remove inorganic toxic anions including nitrate and chromate from aqueous environmental or industrial systems [3,9]. Unfortunately, the achieved sorption capacities of porous LDHs were only able to approach the efficiency of non-porous counterparts [9]. Despite the fact that numerous hard (e.g., solid particles) or soft (e.g., surfactants) template-based processes have been developed to build up porous LDHs, significant increase in the sorption capacity was not achieved. This tendency might be attributed to two issues. First, the templates were not removed from the final materials and thus, the availability of the ion-exchange sites were limited [9]. Second, the presence of macropores lead to formation of hollow spheres [10] around the template and this resulted in a significant decrease in the microporous surface area [11].

Surfactant-mediated preparation of porous LDHs attracted widespread attention in the scientific community in the recent past, since these amphiphilic molecules showed high affinity to LDH surfaces leading to their intercalation and subsequent increase in the distance between the lamellae [12–14]. Among surfactants, sodium dodecyl sulfate (SDS) was extensively used for this purpose [15–17]. Such a pillared structure facilitates the diffusion of the target ions into the interlayer gallery and thus, higher ion-exchange capacity can be achieved. Therefore, LDHs intercalated with SDS were widely used in environmental processes to remove ionic contaminants [16–20] and in the preparation of LDH-based functional materials by immobilization of small molecules of thermoresponsive [12], photoluminescent [21] or hydrophobic [22] properties. The more accessible space is also beneficial once the aim is to attach larger polymeric molecules between the layers [6,23–25].

In these studies, it was confirmed that SDS adsorbed strongly on the oppositely charged surface, and single-molecule adsorption occurred at low concentrations, SDS aggregates formed at higher coverage, while the LDH surface became saturated with the adsorbed SDS around the critical micelle concentration (CMC), which was reported to be around 8 mM [26–28]. Adsorption of SDS at higher concentrations may also reverse the sign of LDH charge leading to the formation of negatively charged SDS-LDH composites [26,29,30]. For instance, the high surfactant affinity was utilized in SDS removal from wastewaters with LDH-titania composites, in which the role of the titania was the photocatalytic decomposition of SDS [31].

Most of the above applications of the SDS-LDH materials took place in dispersions, where possible aggregation of the particles may play an important role, since the aggregates often sediment and hence, the available surface area dramatically decreases. Moreover, surface charge and aggregation processes are strongly related properties of colloidal particles including LDHs [32], therefore, SDS adsorption significantly affects the colloidal stability of the samples. Despite the importance of this issue, systematic studies reporting surface charge densities and aggregation rates of SDS-modified LDHs cannot be found in the literature. The obtained pillared SDS-LDH composites usually possessed high surface area compared to the ones containing small inorganic anions [16,26,33]; however, the organic content of these materials prevents their use in certain applications, e.g., in biological systems. Therefore, SDS removal without sacrificing the high specific surface area would be beneficial, but this topic was rarely investigated in the past.

In the present work, a colloid approach was used to obtain fine dispersions of SDS-LDH composites followed by their calcination to layered double oxide (LDO) to eliminate the SDS content. The organic content-free LDH structure was reconstructed by rehydration of the LDO. The charging and aggregation processes in the SDS-LDH dispersions were optimized in electrophoretic and dynamic light scattering experiments, while the structural features were investigated by electron microscopy, X-ray diffraction, IR spectroscopy, specific surface area and pore size measurements. To demonstrate the sorption ability of the obtained mesoporous materials, the efficiency in removal of dichromate and nitrate anions from aqueous samples was assessed and the adsorption kinetics were analyzed by appropriate models.

2. Materials and method

2.1. Chemicals

All the AR-grade chemicals were purchased from Merck and Sigma-Aldrich and used as received without further purification. More specific data are given in the Supplementary material (SM).

2.2. Synthesis of the pristine MgAl–Cl–LDH

The co-precipitation method [34] was applied, in which 3.0 M NaOH solution was added to a vigorously stirred and N_2-blanketed solution of $MgCl_2$ and $AlCl_3$ of 3:1 M ratio at room temperature. The solid material formed was filtered, dried for 24 h at 60 °C and kept in a desiccator under N_2 until its use in Method 1, as described below.

2.3. Preparation of mesoporous LDH

Method 1. 100.0 mL of 3.0/10.0/30.0 mM sodium dodecyl sulfate (SDS) aqueous solutions were prepared and added to the

MgAl–Cl–LDH dispersions containing 5 g solid material. The samples obtained after SDS adsorption are denoted as SDS_3-MgAl–Cl–LDH, SDS_{10}-MgAl–Cl–LDH and SDS_{30}-MgAl–Cl–LDH, respectively. The slurries were stirred at pH ~ 8.5 (set by 0.015 M NaOH aqueous solution) and 60 °C for 12 h. The solid material was filtered off, washed with distilled water several times and dried at 60 °C overnight. The SDS content was removed by calcination at 510 °C for 12 h leading to the formation of LDO compounds (LDO_3, LDO_{10} and LDO_{30}, respectively). The LDH structures were reconstructed by rehydration, in which the LDOs were dispersed in 100.0 cm^3 of 20.0 mM NaCl dissolved in mixtures of H_2O/EtOH/0.015 M NaOH aqueous solution of 85:5:10 vol ratio under N_2 atmosphere. The slurries were stirred at 50 °C for 96 h followed by repeated filtration, washing (with water) and drying steps to obtain the LDH_3 (from SDS_3-MgAl–Cl–LDH), LDH_{10} (from SDS_{10}-MgAl–Cl–LDH) and LDH_{30} (from SDS_{30}-MgAl–Cl–LDH) final products.

Method 2. During the co-precipitation of LDH in the presence of SDS, 100.0 mL of SDS solutions of 3.0/10.0/30.0 mM concentration were mixed with 50.0 cm^3 aqueous solutions containing 15.0 mM of $MgCl_2$ and 5.0 mM of $AlCl_3$. The pH was kept at 10.5 by addition of 3 M NaOH. After 12 h stirring at 60 °C, the obtained solid materials were separated by filtration, washed with water several times and dried at 60 °C overnight. The solids formed are denoted as c-SDS_3-MgAl–Cl–LDH, c-SDS_{10}-MgAl–Cl–LDH and c-SDS_{30}-MgAl–Cl–LDH and the numbers refer to the concentration of the surfactant during co-precipitation. Like in Method 1, the SDS content was removed by calcination at 510 °C for 12 h leading to LDO formation, which was again transformed to LDH by rehydration. The obtained final materials are denoted as c-LDH_3, c-LDH_{10} and c-LDH_{30}, in respect to SDS dose used in the synthesis.

2.4. Characterization techniques

Electrophoretic mobility was measured with a LiteSizer 500 (Anton Paar) device equipped with a 40 mW laser source operating at 658 nm wavelength. Disposable plastic omega-shaped capillary cells (Anton Paar) were used for the measurements. Conversion method of mobilities to zeta potentials and further data treatment are described in the SM.

Dynamic light scattering (DLS) was used to measure the hydrodynamic size of the dispersed particles. The measurements were carried out with the same LiteSizer device as above at 175° scattering angle in disposable plastic cuvettes (VWR). The cumulant method was used to fit the correlation functions, which were collected for 20 s to determine the hydrodynamic radii of the particles. To assess the colloidal stability of the dispersions, the apparent aggregation rates were measured and used to calculate stability ratios, as detailed elsewhere [35] and in the SM. Note that stability ratios close to unity indicate rapid particle aggregation and unstable dispersions, while higher values refer to more stable samples.

X-ray diffraction (XRD) patterns were recorded on a Rigaku XRD-MiniFlex II instrument applying Cu Kα radiation of 0.15418 nm wavelength with 40 kV accelerating voltage at 30 mA.

The morphologies of the samples prepared were studied by scanning electron microscopy (SEM). The SEM images were recorded on an S-4700 electron microscope (Hitachi) with an accelerating voltage of 10–18 kV. More detailed images on the samples prepared were captured by transmission electron microscopy (TEM). For these measurements, a FEI Tecnai™ G2 20 X-Twin type instrument was used operating at acceleration voltage of 200 kV. The materials were imaged in dried stage by both techniques.

BET (Brunauer-Emmett-Teller) N_2-sorption experiments were carried out on a NOVA3000 (Quantachrome) instrument. The samples were degassed with N_2 at 100 °C for 5 h under vacuum to clean the surface of the adsorbent materials. The measurements were performed at the temperature of liquid N_2.

IR spectra were measured on a BIO-RAD Digilab Division FTS-65A/896 apparatus, equipped with a diffuse reflectance spectroscopy (DRS) accessory. In a typical measurement, 256 scans were collected with 4 cm^{-1} resolution in the 4000–600 cm^{-1} wavenumber range.

2.5. Assessment of sorption capacity

For the nitrate adsorption study, 50 mg of LDH samples were suspended in 10.0 mL solutions containing 5–625 mg/L nitrate anions at room temperature. The samples were continuously stirred at pH 7.0 for 120 h. After the reaction terminated, 1 mL aliquots were filtered with a 0.22 μm membrane filter, and the concentration of nitrate ions in the filtrate was determined by UV–Vis spectrophotometry (Shimadzu UV-1650). For the dichromate adsorption, appropriate amount of $K_2Cr_2O_7$ was dissolved in 100.0 mL of water and the pH was adjusted to 5.0 by adding appropriate amount of NH_4OH solution. Thereafter, 100.0 mg of LDH materials was added into the solution. The reaction time (5–240 min) and the initial concentration of dichromate ion (5–1400 mg/L) were altered. An aliquot of the sample was filtered after 120 h, and the concentration of the dichromate in the filtrate was measured by UV–Vis spectrometry (Shimadzu UV-1650). The error of these methods is about 3%.

The absorbents were regenerated by dispersing the used LDH compounds in 3 M NaCl aqueous solutions, which were vigorously stirred for 12 h. The slurry was then filtered by 0.45 μm membrane filter, washed with water several times and dried at 65 °C overnight. See SM for more details of the evaluation of sorption capacity measurements.

3. Results and discussion

To prepare the mesoporous LDH materials, SDS_3-MgAl–Cl–LDH, SDS_{10}-MgAl–Cl–LDH and SDS_{30}-MgAl–Cl–LDH composites were obtained with Method 1 at different surfactant-to-LDH ratios. Subsequently, they were calcined to the form of LDO and rehydrated to LDH_3, LDH_{10} and LDH_{30}. Extensive structural characterization was performed to explore the correlation between the structure of the obtained materials and the reaction conditions, especially the colloid stability of the precursors. For comparison, c-LDH_3, c-LDH_{10} and c-LDH_{30} materials were prepared by Method 2 using the standard co-precipitation technique. Finally, the adsorption efficiencies were probed by the removal of inorganic anions from aqueous samples.

3.1. Stability of SDSx-MgAl–Cl–LDH dispersions

Surface charge density of +0.5 mC/m^2 was determined for the pristine MgAl–Cl–LDH on the basis of zeta potential measurements (Fig. S1), which were evaluated by the Debye-Hückel model [36] (see SM for the details of the calculation). Such a low charge was accompanied with low critical coagulation concentration of 7 mM, as determined in DLS measurements. These values are typical for LDH colloids containing small inorganic charge compensating anions [32].

Thereafter, in the colloidal approach applied to optimize the synthetic conditions of mesoporous LDHs, the optimal SDS concentrations were explored. Accordingly, the charging and aggregation processes of MgAl–Cl–LDH were followed at different SDS concentrations. Zeta potential measurements were carried out, and slightly positive values were recorded at low SDS doses due to the moderate positive structural charge of the particles (Fig. 1)

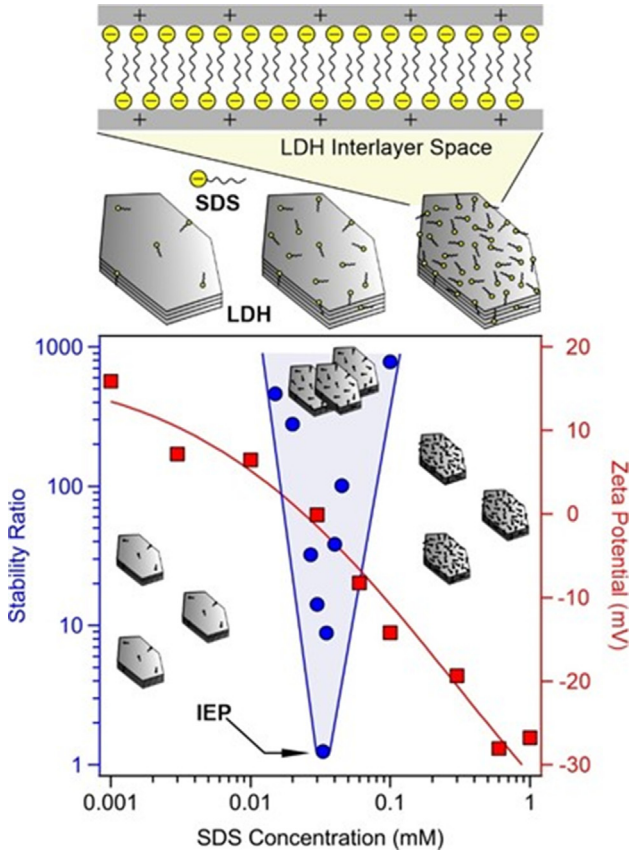

Fig. 1. Zeta potentials (squares, right axis) and stability ratios (circles, left axis) of MgAl–Cl–LDH particles as a function of the SDS concentration in aqueous dispersions at 10 mg/L particle concentration and pH 7. The solid lines are eye guides, and the upper scheme illustrates the SDS bilayer formation between the lamellae. Note that stability ratio close to unity refers to rapid particle aggregation and unstable dispersion.

[37]. Increasing the concentration of SDS, the mobilities decreased indicating surfactant adsorption on the oppositely charged MgAl–Cl–LDH surface. The adsorption process led to charge neutralization at the isoelectric point (IEP) and overcharging at higher doses. Such a reversal in the sign of the charge has been already reported for LDH materials in the presence of strongly adsorbing monovalent ions [38] including SDS [26,30]. The SDS adsorption continued until highly negative zeta potential values.

Colloidal stability was assessed in time resolved DLS measurements under the same experimental conditions as in the mobility study. In unstable samples, the hydrodynamic radii increased with time due to particle aggregation (Fig. S2). From these plots, stability ratios were calculated, as detailed in the SM.

Comparing the tendency in the charging and aggregation data shown in Fig. 1, it is obvious that the charging behavior significantly affects the speed of aggregation. The MgAl–Cl–LDH forms stable dispersion below the IEP, where it possesses significant positive charge due to the small amount of adsorbed SDS. Besides, at elevated SDS concentrations, at which the particles are highly negatively charged, the dispersions are stable again. In contrast, the samples are unstable once the overall charge of the particles is zero at the IEP. These results clearly indicate that the major interparticle forces are of electrostatic origin, in line with the classical theory by Derjaguin, Verwey, Landau and Overbeek [39,40]. Similar charge-aggregation relations were also observed in other nanoparticle systems [32,41].

During the synthesis by Method 1, the MgAl–Cl–LDH concentration was 100 times higher compared to the experiments shown in Fig. 1, therefore, SDS concentrations of 3.0/10.0/30.0 mM were used leading to the formation of SDS_3-MgAl–Cl–LDH, SDS_{10}-MgAl–Cl–LDH and SDS_{30}-MgAl–Cl–LDH composites. The first one forms an unstable dispersion, since the SDS dose is close to the IEP, the second one is just slightly above the CMC of SDS [26] and the final one is at high zeta potential (Fig. 1), where the surface of the MgAl–Cl–LDH is largely negatively charged due to SDS adsorption. In the latter case, the SDS_{30}-MgAl–Cl–LDH forms highly stable colloid.

3.2. Structural features of SDSx-MgAl–Cl–LDH

The XRD patterns of the SDS_3-MgAl–Cl–LDH, SDS_{10}-MgAl–Cl–LDH and SDS_{30}-MgAl–Cl–LDH and the unmodified MgAl–Cl–LDH are presented in Fig. 2. The resulting structure of the latter one is consistent with a rhombohedral unit cell, which is analogous to chloride-containing MgAl–LDHs (see JCPDS#51-1528 database) [42]. Similarly, (003) and (006) Bragg reflections were also observed for the SDS-treated composites. However, more pronounced staging effect was observed with increasing the SDS concentration indicating the presence of a new LDH phase. This is clearly confirmed by the appearance of (003′) and (006′) as well as by the disappearance of (003) bands on increasing the SDS concentration. This phenomenon was observed earlier in other SDS-LDH systems too [13,30]. A new peak appeared around 20° at higher SDS loadings, which originates from the joint effect of complex multiple staging and the different water content [43].

The interlayer distances were calculated with Bragg's equation [44] (see SM for details), and its value was 0.77 nm for the SDS_3-MgAl–Cl–LDH, similarly to other chloride-containing LDHs [45]. Nevertheless, the coexistence of (003) and (003′) peaks indicates two-phase materials of 0.77 and 2.52 nm distances in the case of SDS_{10}-MgAl–Cl–LDH. Only the (003′) diffraction with an interlayer distance of 2.76 nm could be detected for SDS_{30}-MgAl–Cl–LDH. These data shed light on that SDS molecules tend to intercalate by increasing the dose. The internalization process could be rationalized with micelles, since the applied SDS concentrations are above the CMC during the synthesis of both SDS_{10}-MgAl–Cl–LDH and SDS_{30}-MgAl–Cl–LDH. However, as shown in the zeta

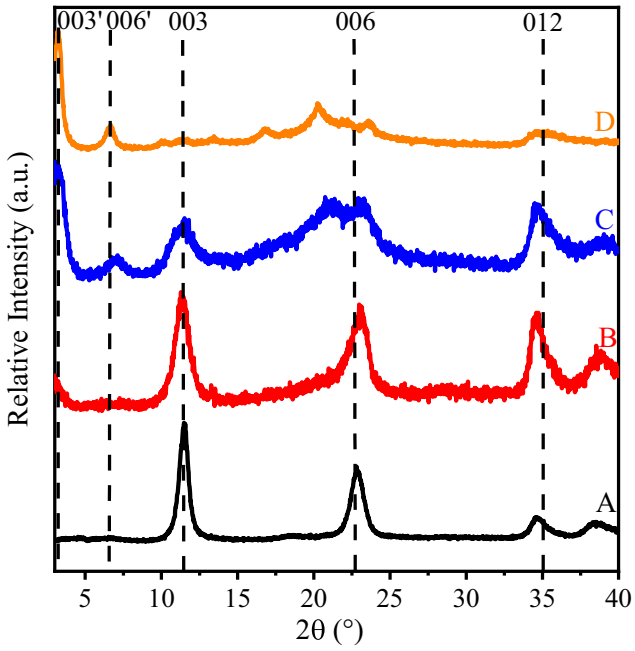

Fig. 2. XRD patterns of (A) MgAl–Cl–LDH, (B) SDS_3–MgAl–Cl–LDH, (C) SDS_{10}–MgAl–Cl–LDH and (D) SDS_{30}–MgAl–Cl–LDH precursor composites prepared by Method 1.

potential study in the previous section, the surfactants are of high affinity to the LDH surface, therefore, DS bilayer formation (illustrated in Fig. 1) in the interlayer space [13] is more feasible.

Recall that the pillared SDS_{30}-MgAl–Cl–LDH is of high negative charge, it forms stable dispersions (Fig. 1), and DS most likely exchanged the majority of chloride ions in the structure. SEM images recorded in dried stage revealed that its morphology was non-defined (Fig. S3A), and it most likely consisted of aggregated particles due to the particle aggregation occurred during the drying process in the SEM measurement.

Besides, very similar XRD patterns were recorded for the materials obtained in the first step of Method 2 (Fig. S4), and they indicate single-phase and non-pillared LDHs. This observation confirmed that no DS intercalation occurred during co-precipitation in Method 2, which was verified by the very similar and small interlayer distances of 0.78, 0.75 and 0.79 nm for c-SDS_3-MgAl–Cl–LDH, c-SDS_{10}-MgAl–Cl–LDH and c-SDS_{30}-MgAl–Cl–LDH, respectively.

Fig. 3 shows the IR spectra of the LDH composites prepared in the first step of by Method 1. All of the SDS modified samples exhibited characteristic bands of DS due to intercalation and adsorption on the outer surface of the MgAl–Cl–LDH. The following peaks were assigned to the DS content: νas(CH) (2922 cm^{-1}), νsym (CH) (2855 cm^{-1}), δ(CH) (1468/1366 cm^{-1}), νas(S=O) (1220 cm^{-1}) and νsym(S=O) (1071 cm^{-1}) (Table S1) [13,33,46,47]. Apart from the vibrational peaks of DS, the bands of the MgAl–Cl–LDH material originating from the surface adsorbed carbonate ions and the water content were also identified.

The IR spectra of the c-SDS_3-MgAl–Cl–LDH, c-SDS_{10}-MgAl–Cl–LDH and c-SDS_{30}-MgAl–Cl–LDH prepared by Method 2 contained the same vibrational bands (Fig. S5) due to the similar chemical composition of the materials. However, DS molecules adsorbed only on the outer surface, as discussed above. By comparing Fig. 3 and Fig. S5, one may realize that the materials prepared by Method 2 contained less carbonate in their structures. This is due to the fact that Method 1 is a more complex process with more time in contact with atmospheric carbon dioxide, which adsorbed in higher extent than during the shorter Method 2.

3.3. LDH-LDO-LDH conversion

In the next step, the SDS-LDH composites were calcined in both Methods 1 and 2 to obtain the corresponding LDO materials forming after the collapse of the LDH structure during the thermal treatment. Results of XRD experiments revealed that the long-range order of LDHs discontinued and amorphous mixed oxides were obtained (Fig. S6). Similar formation of LDO by LDH dehydration has already been reported in the literature [48–51].

To recover the LDH-like structures, the LDO compounds were rehydrated in water-ethanol-NaOH-NaCl solutions in both Methods 1 and 2. The successful reconstruction was confirmed by XRD (Fig. 4 and Fig. S7) by detecting the characteristic pattern for LDH structures [37]. Indeed, single-phase LDHs of similar structures were obtained. On the basis of the interlayer distances, incorporation of chloride (from the rehydrating solution) and/or carbonate (from atmospheric carbon dioxide) anions were assumed.

To further study the structure of the LDH materials, especially the nature of the interlayer space, IR measurements were carried out. The same IR spectra were recorded within the experimental error for all LDHs (Fig. S8), irrespective to the preparation method applied. Two types of characteristic absorption bands were identified in these spectra. First, the ones centered at 1426 and 992 cm^{-1} were assigned to ν3 and ν2 vibration modes of surface-adsorbed carbonate ions. Second, the peaks located at 3535 and 1638 cm^{-1} were assigned to the ν and β vibration modes of the water content. More importantly, not even trace amounts of organic compounds were detected. This result clearly confirms that the SDS template (i.e., intercalated DS anion) was completely eliminated during calcination leading to the formation of template-free LDH materials after rehydration.

Comparing the SEM images of the SDS_{30}-MgAl–Cl–LDH (Fig. S3A) and LDH_{30} (Fig. S3B) materials (i.e., LDH with adsorbed SDS at a dose of 30 mM and the one after rehydration without any SDS), the difference in the morphology is striking. The former one consists of aggregated particles of non-defined structure, while

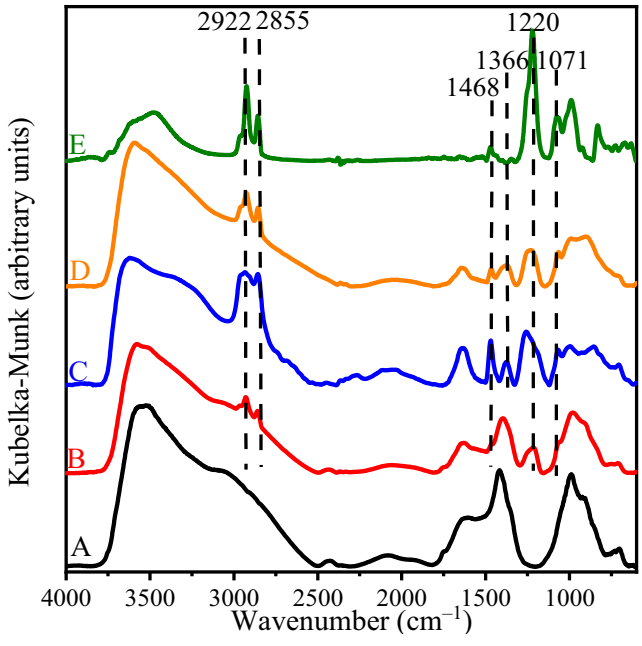

Fig. 3. IR–DRS spectra of (A) MgAl–Cl–LDH, (B) SDS_3-MgAl–Cl^-–LDH, (C) SDS_{10}-MgAl–Cl–LDH, (D) SDS_{30}-MgAl–Cl–LDH and (E) SDS.

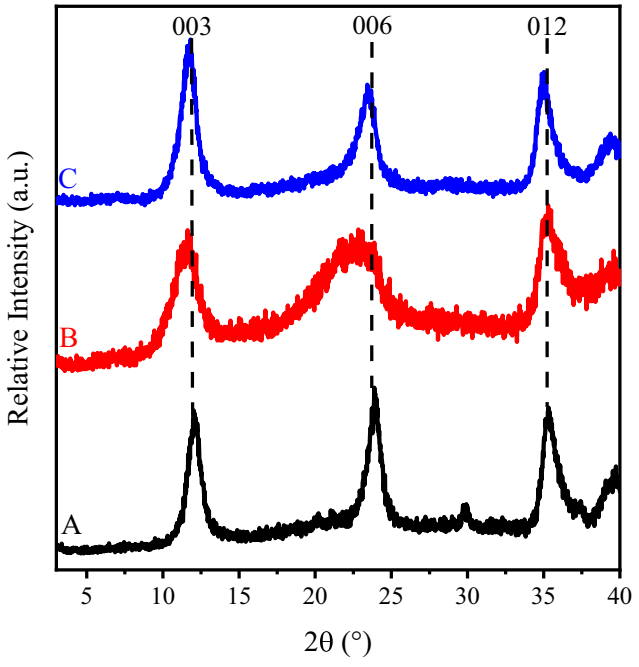

Fig. 4. XRD patterns of (A) LDH_3, (B) LDH_{10} and (C) LDH_{30} obtained after rehydration of LDO_3, LDO_{10} and LDO_{30}, respectively, during Method 1.

the latter one composed of cauliflower-like morphology indicating a highly porous hierarchical structure.

Furthermore, mesoporous holes with different widths were observed on the TEM images of certain LDHs prepared by Method 1 (Fig. 5). Such a tendency to form mesopores was more pronounced by increasing the SDS dose during the synthesis. This issue will be further explored later in the specific surface area assessment. Another interesting finding is that LDH nanosheets stayed in vertically on the cavities suggesting the possible location of an LDH shell around the template before calcination. Nevertheless, similar mesoporous structure was not found in the TEM image of the LDH_3 (Fig. 5A) and of the other LDHs prepared by Method 2 (c-LDH_3, c-LDH_{10} and c-LDH_{30} in Fig. S9A, Fig. S9B and Fig. S9C, respectively). In these cases, the obtained materials were identified as ordinary LDH structures with particle aggregates, in which the sheets arranged vertically around a supposed nodule [52].

Indeed, hierarchical structure was already observed for LDH_{10} (Fig. 5B), but it was the most pronounced for LDH_{30} (Fig. 5C) indicating that the high colloidal stability of the precursor c-SDS_{30}-MgAl–Cl–LDH plays important role in the formation of the materials in the calcination and rehydration steps. The successful application of the colloid chemistry-based design was justified by the advantageous structure of the LDH_{30}.

3.4. Porosity assessment

To receive quantitative information on the porosity of the obtained LDHs, BET measurements were carried out. As the most

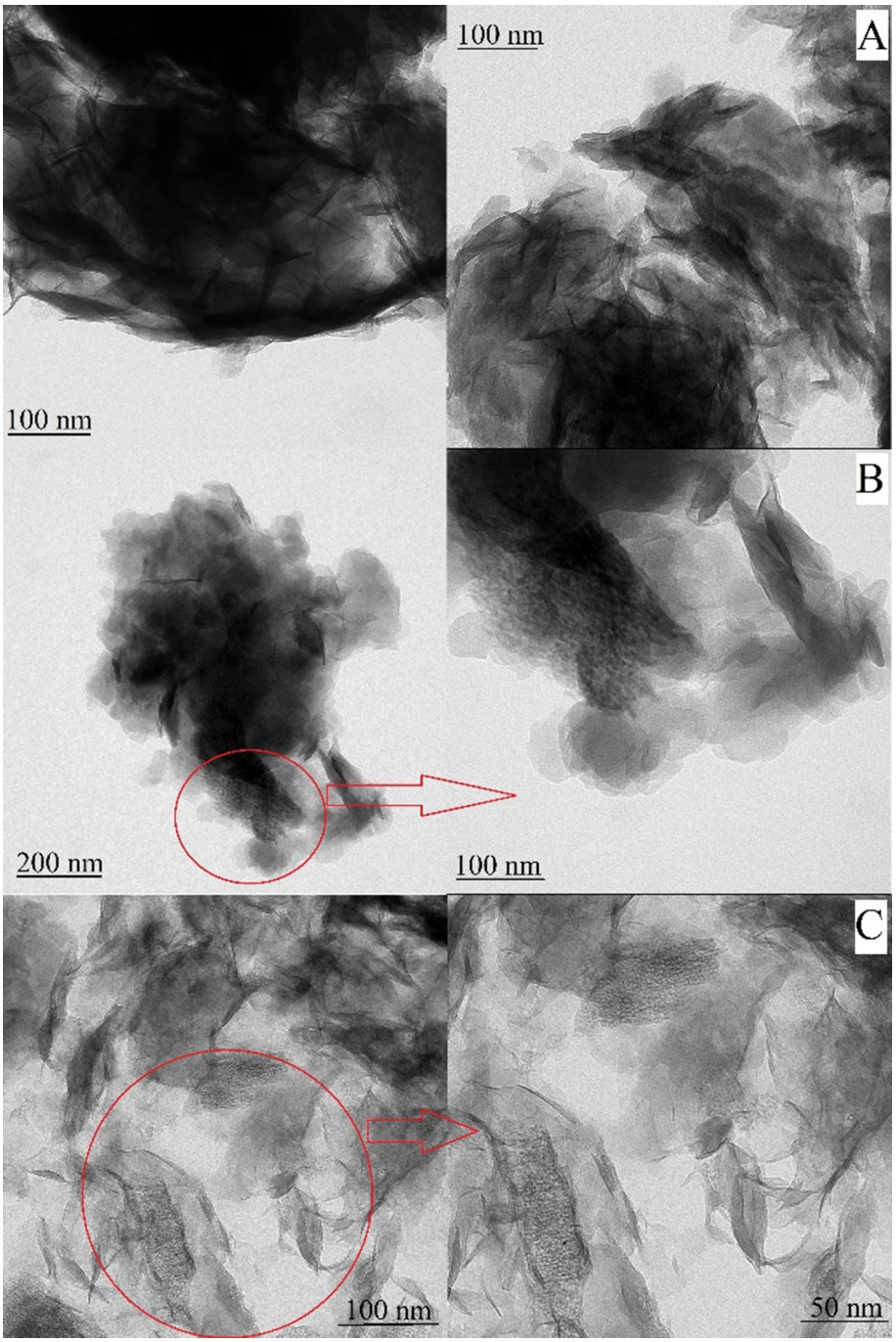

Fig. 5. TEM images of (A) LDH_3, (B) LDH_{10} and (C) LDH_{30} prepared by Method 1.

important factors, specific surface area and pore diameter distribution were determined in N_2-adsorption/desorption measurements (Fig. 6 and Fig. S10A). It was found that almost all of the rehydrated structures exhibited type IV isotherm with H_3 type hysteresis loop (p/p0 > 0.4) indicating the presence of mesopores [53]. However, this type of isotherm and hysteresis loop are typical for plate-like particles of slit shape pores [54]. This feature is usually related to particle aggregates.

On the other hand, rehydrated composites made by Method 1 with high amount of SDS (LDH_{30}) or Method 2 with low amount of SDS (c-LDH_3) exhibited much slower N_2 desorption profile attributed to the presence of thinner nanoplatelets and more mesopores compared to chloride-containing LDHs [55]. For LDH_{30}, the detected hysteresis loop, grouped in H_2 hysteresis, indicates desorption limitation, which is related to the appearance of pores of narrow size distributions and relatively uniform channel, similar to pores with facile pore connectivity [56,57].

Surface area and pore volume values significantly increased in the LDH_3 < LDH_{10} < LDH_{30} order (Fig. 7 and Table S2) indicating that increasing the SDS concentration during the synthesis in Method 1 gives rise to a more porous and hierarchical structure. An important note that the surface area and total pore volume was much higher for LDH_{30} than for c-LDH_{30}, which can be attributed to the significantly different morphology shown in the SEM images (Fig. 7 inset). Accordingly, the compact and aggregated structure for the latter one leads to lower porosity than for the cauliflower-like structure in the case of LDH_{30}.

If one compares the data for MgAl–Cl–LDH and LDH_{30}, 8-time and 48-time increases can be observed in the surface area and total pore volume, respectively. These results are in line with the SEM (Fig. S3B and Fig. 7) and TEM (Fig. 5C) images of LDH_{30}, in which, the highly ordered mesoporous structure is well presented. This result is remarkable, and the determined values are close or even higher than the ones ever reported for LDH materials after synthetic template removal (see a comprehensive set of previously published data in Table S3) [10,58,59].

Typically, the obtained LDH structures give a complete mesopore distribution in the range of 3.5–50.0 nm, depending on the synthesis conditions. The main difference between the pore diameter repartition of LDH materials obtained with Method 1 (Fig. 8) and Method 2 (Fig. S10B) is that only pores of around 4 nm sizes were detected for c-LDH_3, c-LDH_{10} and c-LDH_{30}, while additional pores of diameters up to 50 nm were observed for the materials prepared by Method 1 (Table S2). Note that pore diameters around 4.0 nm might be partially related to the tensile strength effect, which may distort this region of the pore size distribution. The

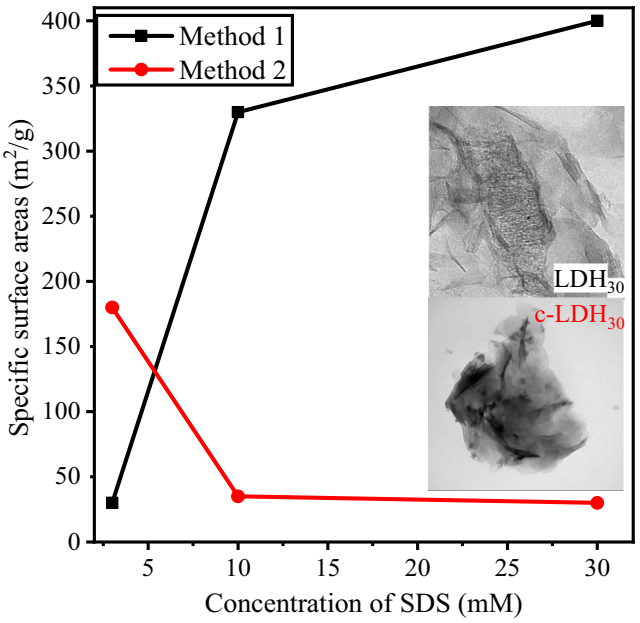

Fig. 7. Specific surface area values as a function of SDS concentration applied in Method 1 (squares) and Method 2 (circles). The TEM images LDH_{30} and c-LDH_{30} are shown in the inset. The lines serve to guide the eyes. The measurement error is typically 5%.

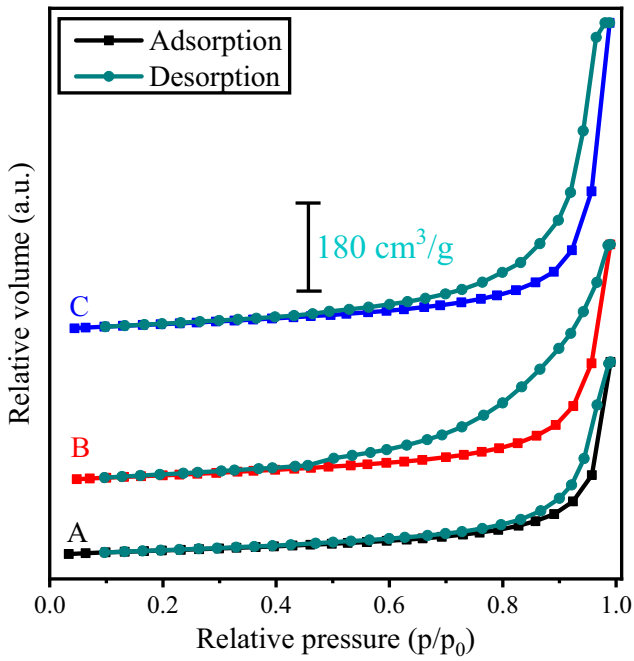

Fig. 6. N_2 sorption isotherms of (A) LDH_3, (B) LDH_{10} and (C) LDH_{30} materials obtained by Method 1.

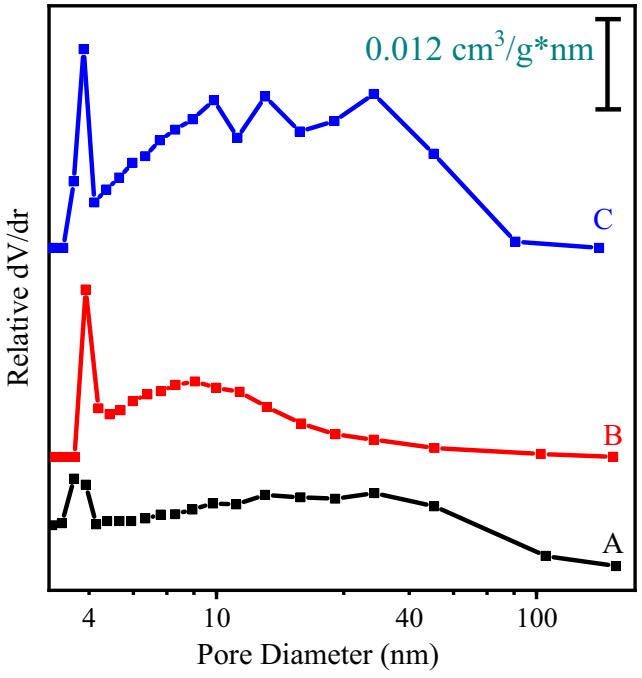

Fig. 8. Pore diameter distribution of (A) LDH_3, (B) LDH_{10} and (C) LDH_{30} materials obtained by Method 1. The data were calculated from the desorption part of the sorption isotherms.

highest value was determined for LDH_{30} indicating that starting from highly charged and stable precursors is the best strategy to obtain such a mesoporous LDH (for comparative data, see Table S3). The obtained high dV/dr values for LDH_3, LDH_{10} and LDH_{30} as well as c-LDH_3 illustrated the formation of hierarchically porous structures [60].

These findings shed light on the important role of SDS adsorption on the MgAl–Cl–LDH material through its effect on the surface charge properties and on the aggregation of the particles. In other words, more porous LDHs or wider pore size distribution can be obtained once the precursor materials (i.e., SDS-LDH hybrid before calcination) are made by adsorption/intercalation of SDS on pristine LDHs, like in Method 1. Moreover, the adsorbed amount and the colloidal stability of the SDS-LDH composites also affect the final structure. Once the feeding material for calcination and subsequent rehydration forms a stable dispersion, then the developed structure shows highly mesoporous and hierarchical features. Accordingly, the most advantageous properties of the final material were obtained, when the highest SDS dose was applied, which condition resulted in homogeneously distributed primary SDS_{30}-MgAl–Cl–LDH particles of high negative charge. In contrast, SDS presence during co-precipitation in Method 2 did not lead to such an advanced feature. Another possible contribution of the intercalated SDS content to the high porosity of the final materials is that its gaseous thermal decomposition products (e.g., sulfur dioxide) carved well-defined pores and channels into the LDHs during calcination. Similar phenomenon was reported earlier in the literature [61–63].

3.5. Efficiency in contaminant removal from water

As a proof of concept, the obtained materials were tested in dichromate and nitrate adsorption experiments. Concerning the former ion, its removal is of great importance for the protection of natural waters from adverse effect of nitrification. On one hand, it is evident that the application of LDHs as anion exchangers should be an efficient solution to solve this problem. On the other hand, it was pointed out that nitrate ions do not attach strongly to the positively charged LDHs and thus, direct anion-exchange reactions were not very successful [64–66].

Therefore, it came as a bit of surprise that our materials showed notable nitrate adsorption (Fig. S11). Let us consider that the amounts of the adsorbed nitrate ions were independent of the applied adsorbent with different porous structure and surface area. Taking into account the relatively low hydrodynamic ionic radius of nitrate anion (2.62 Å), the more porous systems might contribute to faster stream of anions, this fact did not influence the adsorption capacity [67]. The amount of the removed ion increased with increase of the concentration of the nitrate ions up to 575 mg/L nitrate ion loading. The maximum amount of adsorbed nitrate was experienced at 104 mg/g LDH concentration.

Besides, the adsorption capacity could be determined by fitting the measured points with the Langmuir isotherm [68] (Fig. S11 and Table S4, see details of calculations in SM). Comparison to the literature data (Table S5), one may notice that the sorption capacity of 749.7 mg/g determined for LDH_{30} is the highest within the single-phase LDH materials applied earlier for nitrate adsorption. To explore the possible intercalation process of nitrate during ion exchange, XRD patterns were recorded at various nitrate concentrations (Fig. S12), and they clearly indicated the staging effect and intercalation of the nitrate ions.

In the second part of the adsorption studies, the dichromate ion, a well-known carcinogenic contaminant, was used as model compound. Under the conditions applied, $Cr_2O_7^{2-}$ was the predominant species in the samples [69]. The time-dependent measurements (Fig. S13) indicates different sorption capacities for LDH_3, LDH_{10} and LDH_{30}, which increased in this order, in line with their specific surface area. The sorption data indicate that the diffusion of dichromate anions could be enhanced by increasing the pore sizes in contrast to nitrate ions, where no differences were observed for LDH_3, LDH_{10} and LDH_{30}. This is due to the higher hydrodynamic radius of dichromate, which prevents its diffusion into smaller pores. This effect led to efficient ion exchange especially for the LDH_{30}.

The sorption isotherms were calculated to determine the capacity of the LDHs in dichromate adsorption. They could be interpreted by both the Langmuir (equation S8 and Fig. 9) and the Freundlich [70] model (equation S9 and Fig. S14). The first method fit slightly better to the experimental data. The parameters of the isotherms are given in Table 1. The determined sorption capacity of the non-modified LDH structure (19.8 mg/g) is in agreement with previously published data (21.0 mg/g) [71]. For the LDH_3, LDH_{10} and LDH_{30} structures, the sorption capacity increased parallel with the surface area and/or total pore volume. Therefore, the LDH_{30} was the most efficient and, to the best of our knowledge, the obtained value (388.5 mg/g) was the highest among the previously published single-phase LDH materials (Table S6) [9,72–74]. More importantly, the sorption capacity obtained for LDH_{30} is also higher than those of the adsorbers usually used for dichromate removal in the industry (Table S7).

Recyclability of absorbers is always an important parameter. To explore this issue, desorption of dichromate ions was carried out in concentrated (3 M) NaCl solutions. Thereafter, the adsorption isotherms were registered again with the regenerated (dichromate-free) materials. Fig. 10 shows the adsorption capacity values obtained during 5 cycles. Only slight decrease (about 8%) was observed after 5 cycles indicating excellent recyclability of LDH_{30}. In comparison, it was reported for MgAl-CO_3–LDH that only 65% of the ion-exchange capacity could be regenerated after five cycles [71].

The dichromate intercalation and the ion exchange during regeneration were investigated by XRD measurements (Fig. S15). The patterns clearly show that dichromate intercalation occurred during the adsorption reaction indicated by the increased interlayer distances. Moreover, they decreased back to the original

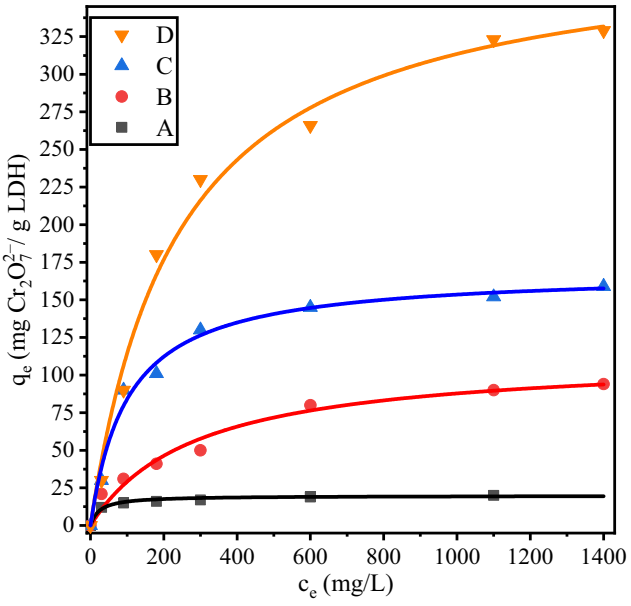

Fig. 9. Dichromate ion adsorption isotherm of (A) MgAl–Cl–LDH, (B) LDH_3, (C) LDH_{10} and (D) LDH_{30}. The solid lines are fits using the Langmuir model.

Table 1
Langmuir and Freundlich isotherm parameters for the adsorption of dichromate ion.

Adsorbent	Langmuir		Freundlich	
	q_m (mg/g)	K_L (*10^{-3} L/mg)	n	K_F (L/g)
MgAl–Cl–LDH	19.8	41.0	2.5	2.0
LDH_3	113.1	3.5	3.7	13.9
LDH_{10}	169.0	9.9	4.8	24.0
LDH_{30}	388.5	0.4	6.3	36.2

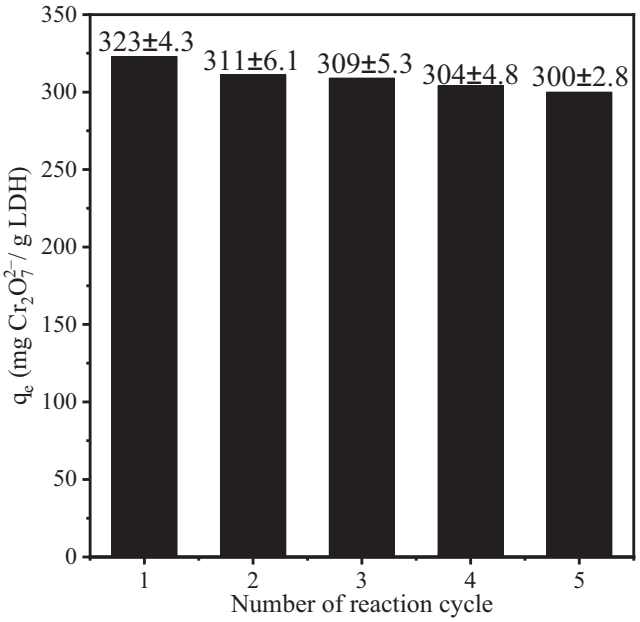

Fig. 10. Regeneration of LDH_{30} adsorbent for 5 consecutive cycles indicated by the adsorption capacities.

value after the regeneration protocol was carried out in NaCl, which shed light on the successful elimination of dichromate.

An interesting information worth mentioning is that the interlayer distance did not change after the anion- exchange reaction in dichromate solutions (Fig. S16). This observation is in contrast with data reported earlier underlining that dichromate (or chromate) intercalation always takes place into LDHs [9,71,75].

4. Conclusions

The present study demonstrates that hierarchical LDH materials of mesoporous features can be obtained with the combined colloid approach. This method relies on the charging and stability assessments of the precursor materials composed of pristine LDH and adsorbed sacrificial SDS molecules on the outer surface and in the interlayer space. Light scattering experiments revealed that SDS adsorption led to charge neutralization and overcharging at appropriate amount of added surfactant. In the latter case, the SDS_{30}–MgAl–Cl–LDH composites formed highly stable colloids. The SDS template was completely removed by calcination to LDO_{30} and the characteristic LDH features were recovered by rehydration to LDH_{30}. For this material, a hierarchical porous structure was obtained. More precisely, 8-time and 48-time increases were detected in the surface area and total pore volume, respectively, in comparison to the case, when template-free LDH material was calcined and rehydrated with the same method.

The LDH structures presented outstanding sorption capacities for both nitrate and dichromate anions with LDH_{30} as the most efficient one. It was pointed out that the adsorbents developed were able to remove nitrate and chromate anions in large quantities by intercalation. To the best of our knowledge, the adsorption capacity of the LDH_{30} sample is the highest among the previously reported LDH materials and superior to several industrially used dichromate removing agents. Furthermore, LDH_{30} showed excellent recyclability.

These advanced properties could be achieved only once the SDS dose is properly adjusted, i.e., the precursor SDS-LDH composite forms highly stable dispersions and surfactant intercalation takes place. Deviation from the optimal amount of SDS gives rise to lower surface area and total pore volumes as well as smaller pore diameters. The results clearly confirm that this novel colloid chemistry approach is a promising way to prepare mesoporous LDHs for applications, wherever organic content-free materials of highly hierarchical internal properties are required.

CRediT authorship contribution statement

Gábor Varga: Investigation, Formal analysis, Visualization. **Zoltán Somosi:** Investigation, Validation. **Zoltán Kónya:** Funding acquisition. **Ákos Kukovecz:** Funding acquisition. **István Pálinkó:** Supervision. **Istvan Szilagyi:** Conceptualization, Funding acquisition, Writing - original draft.

Declaration of Competing Interest

The authors declare that they have no known competing financial interests or personal relationships that could have appeared to influence the work reported in this paper.

Acknowledgements

Financial support by the Ministry of Human Capacities (20391-3/2018/FEKUSTRAT) and by the Hungarian National Research, Development and Innovation Office (SNN 131558) is gratefully acknowledged. G. Varga thanks for the postdoctoral fellowship under the grant PD 128189. The support from the University of Szeged Open Access Fund (4929) is gratefully acknowledged.

Appendix A. Supplementary material

Supplementary data to this article can be found online at https://doi.org/10.1016/j.jcis.2020.08.118.

References

[1] Z.B. Cao, B. Li, L.Y. Sun, L. Li, Z.P. Xu, Z. Gu, 2D layered double hydroxide nanoparticles: recent progress toward preclinical/clinical nanomedicine, Small Methods (2019) 1900343.
[2] F. Song, L.C. Bai, A. Moysiadou, S. Lee, C. Hu, L. Liardet, X.L. Hu, Transition metal oxides as electrocatalysts for the oxygen evolution reaction in alkaline solutions: an application-inspired renaissance, J. Am. Chem. Soc. 140 (2018) 7748–7759.
[3] K.H. Goh, T.T. Lim, Z. Dong, Application of layered double hydroxides for removal of oxyanions: a review, Water Res. 42 (2008) 1343–1368.
[4] P.J. Sideris, U.G. Nielsen, Z.H. Gan, C.P. Grey, Mg/Al ordering in layered double hydroxides revealed by multinuclear NMR spectroscopy, Science 321 (2008) 113–117.

[5] Z. Gu, J.J. Atherton, Z.P. Xu, Hierarchical layered double hydroxide nanocomposites: structure, synthesis and applications, Chem. Commun. 51 (2015) 3024–3036.
[6] F. Leroux, J.P. Besse, Polymer interleaved layered double hydroxide: a new emerging class of nanocomposites, Chem. Mat. 13 (2001) 3507–3515.
[7] Z. Gu, A.C. Thomas, Z.P. Xu, J.H. Campbell, G.Q. Lu, In vitro sustained release of LMWH from MgAl-layered double hydroxide nanohybrids, Chem. Mat. 20 (2008) 3715–3722.
[8] K.H. Goh, T.T. Lim, Z.L. Dong, Enhanced arsenic removal by hydrothermally treated nanocrystalline Mg/Al layered double hydroxide with nitrate intercalation, Environ. Sci. Technol. 43 (2009) 2537–2543.
[9] H.P. Chao, Y.C. Wang, H.N. Tran, Removal of hexavalent chromium from groundwater by Mg/Al-layered double hydroxides using characteristics of in-situ synthesis, Environ. Pollut. 243 (2018) 620–629.
[10] M.F. Shao, F.Y. Ning, Y.F. Zhao, J.W. Zhao, M. Wei, D.G. Evans, X. Duan, Core-shell layered double hydroxide microspheres with tunable interior architecture for supercapacitors, Chem. Mat. 24 (2012) 1192–1197.
[11] H.S. Ji, W.H. Wu, F.H. Li, X.X. Yu, J.J. Fu, L.Y. Jia, Enhanced adsorption of bromate from aqueous solutions on ordered mesoporous Mg-Al layered double hydroxides (LDHs), J. Hazard. Mater. 334 (2017) 212–222.
[12] G. Abellan, J.L. Jorda, P. Atienzar, M. Varela, M. Jaafar, J. Gomez-Herrero, F. Zamora, A. Ribera, H. Garcia, E. Coronado, Stimuli-responsive hybrid materials: breathing in magnetic layered double hydroxides induced by a thermoresponsive molecule, Chem. Sci. 6 (2015) 1949–1958.
[13] P. Zhang, G.R. Qian, Z.P. Xu, H.S. Shi, X.X. Ruan, J. Yang, R.L. Frost, Effective adsorption of sodium dodecylsulfate (SDS) by hydrocalumite (CaAl-LDH-Cl) induced by self-dissolution and re-precipitation mechanism, J. Colloid Interface Sci. 367 (2012) 264–271.
[14] J. Zhang, X.L. Xie, C.J. Li, H. Wang, L.J. Wang, The role of soft colloidal templates in the shape evolution of flower-like MgAl-LDH hierarchical microstructures, RSC Adv. 5 (2015) 29757–29765.
[15] L. Fernandez, I. Ledezma, C. Borras, L.A. Martinez, H. Carrero, Horseradish peroxidase modified electrode based on a film of Co-Al layered double hydroxide modified with sodium dodecylbenzenesulfonate for determination of 2-chlorophenol, Sens. Actuator B-Chem. 182 (2013) 625–632.
[16] L. Deng, H.X. Zeng, Z. Shi, W. Zhang, J.M. Luo, Sodium dodecyl sulfate intercalated and acrylamide anchored layered double hydroxides: a multifunctional adsorbent for highly efficient removal of Congo red, J. Colloid Interface Sci. 521 (2018) 172–182.
[17] Y. Kong, Y.R. Huang, C. Meng, Z. Zhang, Sodium dodecylsulfate-layered double hydroxide and its use in the adsorption of 17-estradiol in wastewater, RSC Adv. 8 (2018) 31440–31454.
[18] H. Chen, G.R. Qian, X.X. Ruan, R.L. Frost, Removal process of nickel(II) by using dodecyl sulfate intercalated calcium aluminum layered double hydroxide, Appl. Clay Sci. 132 (2016) 419–424.
[19] S.T. Lin, H.N. Tran, H.P. Chao, J.F. Lee, Layered double hydroxides intercalated with sulfur-containing organic solutes for efficient removal of cationic and oxyanionic metal ions, Appl. Clay Sci. 162 (2018) 443–453.
[20] P. Zhang, S.D. Ouyang, P. Li, Y. Huang, R.L. Frost, Enhanced removal of ionic dyes by hierarchical organic three-dimensional layered double hydroxide prepared via soft-template synthesis with mechanism study, Chem. Eng. J. 360 (2019) 1137–1149.
[21] J. Xu, D.P. Yan, S.D. Li, J. Lu, Controllable luminescence and electrochemical detection of Pb^{2+} ion based on the 2,2 '-Azino-bis(3-ethylbenzothiazoline-6-sulfonate) dye and dodecanesulfonate co-intercalated layered double hydroxide, Dyes Pigment. 94 (2012) 74–80.
[22] Q. Tao, H.P. He, R.L. Frost, P. Yuan, J.X. Zhu, Nanomaterials based upon silylated layered double hydroxides, Appl. Surf. Sci. 255 (2009) 4334–4340.
[23] Q.Q. Chen, M.X. Nie, Y. Guo, Controlled synthesis and humidity sensing properties of CdS/polyaniline composite based on CdAl layered double hydroxide, Sens. Actuator B-Chem. 254 (2018) 30–35.
[24] T. Wu, Q.H. Kong, H.K. Zhang, J.H. Zhang, Thermal stability and flame retardancy of polypropylene/NiAl layered double hydroxide nanocomposites, J. Nanosci. Nanotechnol. 18 (2018) 1051–1056.
[25] Q.H. Kong, T. Wu, J.Q. Wang, H. Liu, J.H. Zhang, Improving the thermal stability and flame retardancy of PP/IFR composites by NiAl-layered double hydroxide, J. Nanosci. Nanotechnol. 18 (2018) 3660–3665.
[26] P.C. Pavan, E.L. Crepaldi, G.D. Gomes, J.B. Valim, Adsorption of sodium dodecylsulfate on a hydrotalcite-like compound. Effect of temperature, pH and ionic strength, Colloid Surf. A 154 (1999) 399–410.
[27] P. Zhang, M.X. Xiang, P. Li, S.D. Ouyang, T. He, Q. Deng, The enhancement roles of sulfate on the adsorption of sodium dodecylsulfate by calcium-based layered double hydroxide: microstructure and thermal behaviors, Environ. Sci. Pollut. Res. 26 (2019) 19320–19326.
[28] P. Zhang, T. He, P. Li, X.Z. Zeng, Y. Huang, New insight into the hierarchical microsphere evolution of organic three-dimensional layer double hydroxide: the key role of the surfactant template, Langmuir 35 (2019) 13562–13569.
[29] P. Zhang, S.D. Ouyang, P. Li, Z. Gu, Y.G. Huang, S. Deng, Effect of anion co-existence on ionic organic pollutants removal over Ca based layered double hydroxide, J. Colloid Interface Sci. 534 (2019) 440–446.
[30] J. Wang, F. Yang, C.F. Li, S.Y. Liu, D.J. Sun, Double phase inversion of emulsions containing layered double hydroxide particles induced by adsorption of sodium dodecyl sulfate, Langmuir 24 (2008) 10054–10061.
[31] F. Aoudjit, O. Cherifi, D. Halliche, Simultaneously efficient adsorption and photocatalytic degradation of sodium dodecyl sulfate surfactant by one-pot synthesized TiO2/layered double hydroxide materials, Sep. Sci. Technol. 54 (2019) 1095–1105.
[32] M. Pavlovic, P. Rouster, T. Oncsik, I. Szilagyi, Tuning colloidal stability of layered double hydroxides: from monovalent ions to polyelectrolytes, ChemPlusChem 82 (2017) 121–131.
[33] J. He, B. Li, D.G. Evans, X. Duan, Synthesis of layered double hydroxides in an emulsion solution, Colloid Surf. A 251 (2004) 191–196.
[34] J. He, M. Wei, B. Li, Y. Kang, D.G. Evans, X. Duan, Preparation of layered double hydroxides, in: X. Duan, D.G. Evans (eds.), Layered Double Hydroxides, 2006, pp. 89–119.
[35] H. Holthoff, S.U. Egelhaaf, M. Borkovec, P. Schurtenberger, H. Sticher, Coagulation rate measurements of colloidal particles by simultaneous static and dynamic light scattering, Langmuir 12 (1996) 5541–5549.
[36] G. Trefalt, I. Szilagyi, M. Borkovec, Poisson-Boltzmann description of interaction forces and aggregation rates involving charged colloidal particles in asymmetric electrolytes, J. Colloid Interface Sci. 406 (2013) 111–120.
[37] D.G. Evans, R.C.T. Slade, Structural aspects of layered double hydroxides, in: X. Duan, D.G. Evans (eds.), Layered Double Hydroxides, 2006, pp. 1–87.
[38] M. Pavlovic, R. Huber, M. Adok-Sipiczki, C. Nardin, I. Szilagyi, Ion specific effects on the stability of layered double hydroxide colloids, Soft Matter 12 (2016) 4024–4033.
[39] B. Derjaguin, L.D. Landau, Theory of the stability of strongly charged lyophobic sols and of the adhesion of strongly charged particles in solutions of electrolytes, Acta Phys. Chim. 14 (1941) 633–662.
[40] E.J.W. Verwey, J.T.G. Overbeek, Theory of Stability of Lyophobic Colloids, Elsevier, Amsterdam, 1948.
[41] J. Song, Y.N. Tan, D. Janczewski, M.A. Hempenius, J.W. Xu, H.R. Tan, G.J. Vancso, Poly(ferrocenylsilane) electrolytes as a gold nanoparticle foundry: "two-in-one" redox synthesis and electrosteric stabilization, and sensing applications, Nanoscale 9 (2017) 19255–19262.
[42] Y.S. Gao, J.W. Wu, Z. Zhang, R. Jin, X. Zhang, X.R. Yan, A. Umar, Z.H. Guo, Q. Wang, Synthesis of polypropylene/Mg_3Al-X (X = CO_3^{2-}, NO_3^-, Cl^-, SO_4^{2-}) LDH nanocomposites using a solvent mixing method: thermal and melt rheological properties, J. Mater. Chem. A 1 (2013) 9928–9934.
[43] S.P. Newman, S.J. Williams, P.V. Coveney, W. Jones, Interlayer arrangement of hydrated MgAl layered double hydroxides containing guest terephthalate anions: Comparison of simulation and measurement, J. Phys. Chem. B 102 (1998) 6710–6719.
[44] W.H. Bragg, W.L. Bragg, The reflection of X-rays by crystals, Proc. R. soc. Lond. Ser. A-Contain. Pap. Math. Phys. Character 88 (1913) 428–438.
[45] N. Iyi, Y. Ebina, T. Sasaki, Water-swellable MgAl-LDH (layered double hydroxide) hybrids: synthesis, characterization, and film preparation, Langmuir 24 (2008) 5591–5598.
[46] N. Iyi, T. Matsumoto, Y. Kaneko, K. Kitamura, Deintercalation of carbonate ions from a hydrotalcite-like compound: enhanced decarbonation using acid-salt mixed solution, Chem. Mat. 16 (2004) 2926–2932.
[47] Y. Sun, Y. Zhou, X. Ye, J. Chen, Z. Wang, Fabrication and infrared emissivity study of hybrid materials based on immobilization of collagen onto exfoliated LDH, Mater. Lett. 62 (2008) 2943–2946.
[48] Z.J. Yuan, S.M. Bak, P.S. Li, Y. Jia, L.R. Zheng, Y. Zhou, L. Bai, E.Y. Hu, X.Q. Yang, Z. Cai, Y.M. Sun, X.M. Sun, Activating layered double hydroxide with multivacancies by memory effect for energy-efficient hydrogen production at neutral pH, ACS Energy Lett. 4 (2019) 1412–1418.
[49] S. Meszaros, J. Halasz, Z. Konya, P. Sipos, I. Palinko, Reconstruction of calcined MgAl- and NiMgAl-layered double hydroxides during glycerol dehydration and their recycling characteristics, Appl. Clay Sci. 80–81 (2013) 245–248.
[50] T. Bujdoso, A. Patzko, Z. Galbacs, I. Dekany, Structural characterization of arsenate ion exchanged MgAl-layered double hydroxide, Appl. Clay Sci. 44 (2009) 75–82.
[51] J.S. Valente, F. Figueras, M. Gravelle, P. Kumbhar, J. Lopez, J.P. Besse, Basic properties of the mixed oxides obtained by thermal decomposition of hydrotalcites containing different metallic compositions, J. Catal. 189 (2000) 370–381.
[52] M.A. Ulibarri, F.M. Labajos, V. Rives, R. Trujillano, W. Kagunya, W. Jones, Comparative-study of the synthesis and properties of vanadate-exchanged layered double hydroxides, Inorg. Chem. 33 (1994) 2592–2599.
[53] H.R. Suo, H.H. Duan, C.P. Chen, J.C. Buffet, D. O'Hare, Bifunctional acid-base mesoporous silica@aqueous miscible organic-layered double hydroxides, RSC Adv. 9 (2019) 3749–3754.
[54] B. Li, Y.X. Zhang, X.B. Zhou, Z.L. Liu, Q.Z. Liu, X.H. Li, Different dye removal mechanisms between monodispersed and uniform hexagonal thin plate-like MgAl-CO32–LDH and its calcined product in efficient removal of Congo red from water, J. Alloy. Compd. 673 (2016) 265–271.
[55] C.P. Chen, M.S. Yang, Q. Wang, J.C. Buffet, D. O'Hare, Synthesis and characterisation of aqueous miscible organic-layered double hydroxides, J. Mater. Chem. A 2 (2014) 15102–15110.
[56] S. Mendioroz, J.A. Pajares, I. Benito, C. Pesquera, F. Gonzalez, C. Blanco, Texture evolution of montmorillonite under progressive acid treatment – change from H-3 to H-2 type of hysteresis, Langmuir 3 (1987) 676–681.
[57] G.H. Zhang, B.Z. Lin, Y.Q. Qiu, L.W. He, Y.L. Chen, B.F. Gao, Highly efficient visible-light-driven photocatalytic hydrogen generation by immobilizing CdSe nanocrystals on ZnCr-layered double hydroxide nanosheets, Int. J. Hydrog. Energy 40 (2015) 4758–4765.
[58] P. Gunawan, R. Xu, Direct assembly of anisotropic layered double hydroxide (LDH) nanocrystals on spherical template for fabrication of drug-LDH hollow nanospheres, Chem. Mat. 21 (2009) 781–783.

[59] J. Li, N. Zhang, D.H.L. Ng, Synthesis of a 3D hierarchical structure of gamma-AlO (OH)/Mg-Al-LDH/C and its performance in organic dyes and antibiotics adsorption, J. Mater. Chem. A 3 (2015) 21106–21115.
[60] R. Pourfaraj, S.J. Fatemi, S.Y. Kazemi, P. Biparva, Synthesis of hexagonal mesoporous MgAl LDH nanoplatelets adsorbent for the effective adsorption of Brilliant Yellow, J. Colloid Interface Sci. 508 (2017) 65–74.
[61] J.M. Patterson, Z. Kortylewicz, W.T. Smith, Thermal-degradation of sodium dodecyl-sulfate, J. Agric. Food Chem. 32 (1984) 782–784.
[62] D. Ramimoghadam, M.Z. Bin Hussein, Y.H. Taufiq-Yap, The effect of sodium dodecyl sulfate (SDS) and cetyltrimethylammonium bromide (CTAB) on the properties of ZnO synthesized by hydrothermal method, Int. J. Mol. Sci. 13 (2012) 13275–13293.
[63] A. Malak-Polaczyk, C. Vix-Guterl, E. Frackowiak, Carbon/layered double hydroxide (LDH) composites for supercapacitor application, Energy Fuels 24 (2010) 3346–3351.
[64] S. Miyata, Anion-exchange properties of hydrotalcite-like compounds, Clay Clay Min. 31 (1983) 305–311.
[65] B.X. Li, J. He, D.G. Evans, X. Duan, Inorganic layered double hydroxides as a drug delivery system - intercalation and in vitro release of fenbufen, Appl. Clay Sci. 27 (2004) 199–207.
[66] G. Varga, A. Kukovecz, Z. Konya, L. Korecz, S. Murath, Z. Csendes, G. Peintler, S. Carlson, P. Sipos, I. Palinko, Mn(II)-amino acid complexes intercalated in CaAl-layered double hydroxide – well-characterized, highly efficient, recyclable oxidation catalysts, J. Catal. 335 (2016) 125–134.
[67] S. Sugiharto, T.M. Lewis, A.J. Moorhouse, P.R. Schofield, P.H. Barry, Anion-cation permeability correlates with hydrated counterion size in glycine receptor channels, Biophys. J. 95 (2008) 4698–4715.
[68] I. Langmuir, The adsorption of gases on plane surfaces of glass, mica and platinum, J. Am. Chem. Soc. 40 (1918) 1361–1403.
[69] F. Brito, J. Ascanio, S. Mateo, C. Hernandez, L. Araujo, P. Gili, P. MartinZarza, S. Dominguez, A. Mederos, Equilibria of chromate(VI) species in acid medium and ab initio studies of these species, Polyhedron 16 (1997) 3835–3846.
[70] H. Freundlich, Über die adsorption in lösungen, Z. Phys. Chem. 57 (1907) 385–470.
[71] S. He, Y.F. Zhao, M. Wei, D.G. Evans, X. Duan, Fabrication of hierarchical layered double hydroxide framework on aluminum foam as a structured adsorbent for water treatment, Ind. Eng. Chem. Res. 51 (2012) 285–291.
[72] N.N. Das, J. Konar, M.K. Mohanta, S.C. Srivastava, Adsorption of Cr(VI) and Se (IV) from their aqueous solutions onto Zr^{4+}-substituted ZnAl/MgAl-layered double hydroxides: effect of Zr^{4+} substitution in the layer, J. Colloid Interface Sci. 270 (2004) 1–8.
[73] V.M. Boddu, K. Abburi, J.L. Talbott, E.D. Smith, Removal of hexavalent chromium from wastewater using a new composite chitosan biosorbent, Environ. Sci. Technol. 37 (2003) 4449–4456.
[74] L. Zhu, Y. Liu, J. Chen, Synthesis of N-methylimidazolium functionalized strongly basic anion exchange resins for adsorption of Cr(VI), Ind. Eng. Chem. Res. 48 (2009) 3261–3267.
[75] N. Tarutani, Y. Tokudome, M. Fukui, K. Nakanishi, M. Takahashi, Fabrication of hierarchically porous monolithic layered double hydroxide composites with tunable microcages for effective oxyanion adsorption, RSC Adv. 5 (2015) 57187–57192.